Journal of Alloys and Compounds 509 (2011) 2611–2616

Contents lists available at ScienceDirect

Journal of Alloys and Compounds

journal homepage: www.elsevier.com/locate/jallcom

Structural, elastic properties and pressure-induced phase transition of 'half-Heusler' alloy CoVSb

Bo Kong[a], Xiang-Rong Chen[a,b,*], Jing-Xin Yu[a], Cang-Ling Cai[c]

[a] College of Physical Science and Technology, Sichuan University, Chengdu 610064, China
[b] International Centre for Materials Physics, Chinese Academy of Sciences, Shenyang 110016, China
[c] Laboratory for Shock Wave and Detonation Physics Research, Institute of Fluid Physics, Chinese Academy of Engineering Physics, Mianyang 621900, China

ARTICLE INFO

Article history:
Received 22 July 2010
Accepted 17 November 2010
Available online 25 November 2010

Keywords:
CoVSb
Elastic properties
Pressure-induced phase transition
Generalized gradient approximation

ABSTRACT

The structural, elastic properties and the pressure-induced phase transition of 'half-Heusler' alloy CoVSb are investigated using the pseudopotential plane wave method within the generalized gradient approximation (GGA). The calculated structural parameters are in good agreement with the available experimental and theoretical data. The elastic constants and their pressure dependences of 'half-Heusler' cubic CoVSb are calculated using the static finite strain technique, and are presented for the first time together with the theoretical pressure-induced phase transition. The research of phase transition and the calculations of electronic structures show that the 'half-Heusler' cubic CoVSb transforms to normal hexagonal CoVSb with atomic configurations I and II at about 13.5 and 78.0 GPa, respectively at 0 K. Combining the analysis of ground-state structures, it is concluded that the 'half-Heusler' cubic CoVSb mainly transforms to hexagonal CoVSb with atomic configuration I at a relative lower pressure.

1. Introduction

Half-Heusler alloys, that open a gap at Fermi level in the energy bands for only one spin direction, have attracted considerable attentions since de Groot et al. studied NiMnSb [1]. For these alloys, the conduction electrons at Fermi level are 100% spin-polarized [2], suggesting that they can be used as electronic devices, e.g. as spin valves, to increase giant magneto-resistance (GMR) [3], or as possible spin injector electrodes in tunnel magneto-resistance (TMR) structures [4,5], or for spin polarized current injection into semiconductors (spintronics) [6], and so on. Apparently, they are very interesting from both theoretical and practical points of view. A lot of studies on their electronic, magnetic and transport properties were reported [1–13].

Usually, the half-Heusler alloys have the form XMZ (X = Fe, Co, Ni, Pt, Au, M = Ti, V, Cr, Mn, Zr, Nb, Mo, and Z = Sn, Sb) [8]. They crystallize in the face-centred cubic MgAgAs-type structure with the space group *F4–3m* (No 216). The M and Z atoms locate at 4*a* (0, 0, 0) and 4*b* (1/2, 1/2,1/2) sites to form the rock salt structure, while the X atom locates in the octahedrally coordinated pocket, at one of the cubic centre site 4*c* (1/4, 1/4, 1/4), leaving the other 4*d* (3/4, 3/4, 3/4) empty (Fig. 1). This is the conventional stable structure for the half-Heusler alloys [11].

In these half-Heusler alloys, CoVSb has initiated a lot of study in term of its some particular physical properties and some disagreements between experiments and theories [7,14–21]. In experiment, its crystal structure was reported for the fist time by Kripyakevich and Markiv [14] in 1963; in 1972, Terada et al. [15] reported cubic structure CoVSb is a weak itinerant ferromagnetic alloy; in 1979, Noda et al. [16] investigated the crystal structure of CoVSb by X-ray at low and high pressures, and found that the cubic CoVSb transforms to hexagonal structure (space group *P63/mmc*, No 164) with two kinds of atomic configurations shown in Fig. 2 at 5 GPa and 1200 K; in 1998, Kaczmarska et al. [17] investigated the magnetization, Hall effect, thermopower, pressure dependence of resistivity and electron spin resonance (ESR) for the cubic CoVSb by a four-probe AC current method, also again investigated its crystal structure by X-ray; in 2005, a striking result from Heyne and coworkers experiment [18] with a SQUID magnetometer was that the cubic CoVSb is not a half-Heusler alloy. However, in theory, all electronic structure calculations of Ishida et al. (the LMTO-ASA method) [7], Tobola et al. (both KKR and KKR-CPA methods) [19], Galanakis and Dederichs (the full-potential screened KKR method within LSDA approximation) [20], Nanda and Dasgupta (the full-potential linearized muffintin orbital method and the tight-binding linearized muffin tin orbital method) [21] showed that the cubic CoVSb is a half-Heusler alloy. On the other hand, the calculated cubic CoVSb magnetic moments of Ishida et al. [7] and Tobola et al. [19] are bigger than the experimental data of Terada et al. [15]. Tobola et al. [19] pointed out that one possible reason for these discrepancies is the atomic disorder between Co and V atoms; V

* Corresponding author at: College of Physical Science and Technology, Sichuan University, Chengdu 610064, China.
E-mail addresses: kong79@yeah.net (B. Kong), x.r.chen@tom.com (X.-R. Chen).

0925-8388/$ – see front matter © 2010 Elsevier B.V. All rights reserved.
doi:10.1016/j.jallcom.2010.11.119

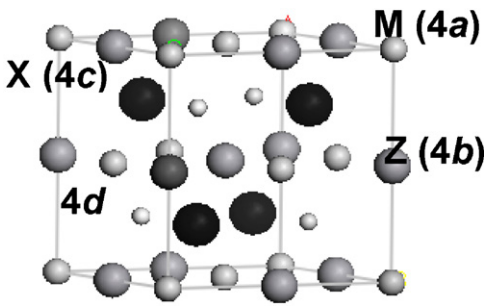

Fig. 1. The crystal structure of cubic half-Heusler alloy XMZ.

atom has a smaller radius than other 3*d* metals which occupy the Y sublattice and is close to that of Co, which may lead to greater disorder. Of course, experiments itself also may have errors. In this work, we mainly focus on other some properties, i.e. the structural, elastic properties and the pressure-induced phase transition of the 'half-Heusler' alloy CoVSb using first-principles calculations. At the same time, we also present some electronic properties that other authors less mentioned. From the calculated cubic CoVSb elastic constants, we will investigate its mechanical stability and anisotropic behavior, the bulk modulus, shear modulus, Young's modulus, shear, longitudinal and average sound velocities, as well as Debye temperature and Poisson's ratio. In Section 2, we give the brief descriptions of theoretical methods. The results of structural, elastic, electronic properties and the pressure-induced phase transition of the 'half-Heusler' alloy CoVSb are presented in Section 3. A summary is given in the last section.

2. Theoretical methods

2.1. Total energy electronic structure calculations

We calculated the electronic structures of cubic and hexagonal CoVSb alloys using the plane-wave pseudopotential density functional theory method through the Cambridge Serial Total Energy Package (CASTEP) code [22,23], together with the generalized gradient approximation (GGA-PBE) [24] for the exchange–correlation function. The Kohn–Sham equation was solved by means of the ultrasoft pseudopotentials introduced by Vanderbilt [25]. Pseudo-atomic calculations were performed for Co $3d^7 4s^2$, V $3s^2 3p^6 3d^3 4s^2$ and Sb $5s^2 5p^3$. A plane-wave basis set with energy cut-off 400 eV was applied. For Brillouin zone sampling, we used $9 \times 9 \times 9$ and $8 \times 8 \times 6$ Monkhorst–Pack meshes for the cubic and hexagonal CoVSb, respectively. The self-consistent convergence of the total energy was 10^{-6} eV/atom. A full optimization of the unit cell structure for each target external pressure was performed using the Broyden–Fletcher–Goldfarb–Shenno (BFGS) minimization technique [26], which provides a fast way of finding the lowest energy structure and the optimized cell at different hydrostatic pressures. More precise testing calculations with cut-off energy of 550 eV have been implemented, and the obtained results showed that the more precise calculations have little influence on the equilibrium lattice constant, energy and enthalpy. But for the calculations of elastic constants of cubic CoVSb, these parameters do not fit. Weighting various factors, we adopted 500 eV cut-off energy and $11 \times 11 \times 11$ Monkhorst–Pack mesh at 0, 5 and 10 GPa; $13 \times 13 \times 13$ Monkhorst–Pack mesh at 15 GPa, so that the convergences of low pressure elastic stiffness coefficients are guaranteed.

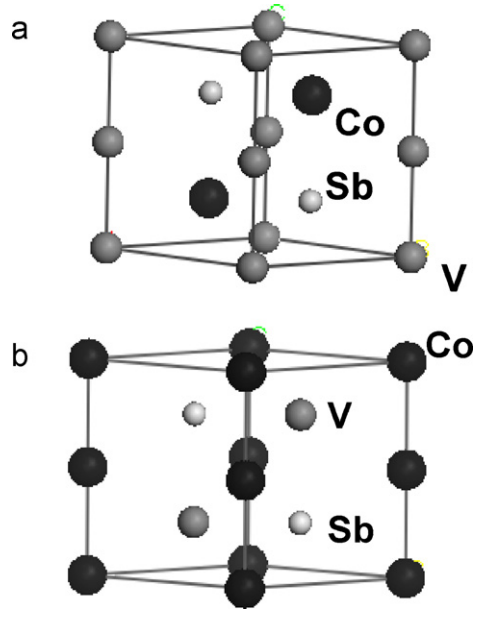

Fig. 2. (a) Hexagonal CoVSb with atomic configuration I: V in 2*a* at (0, 0, 0) and Co in 2*d* at (1/3, 2/3, 3/4) and Sb in 2*c* at (1/3, 2/3, 1/4); (b) hexagonal CoVSb with atomic configuration II: V in 2*d* at (1/3, 2/3, 3/4) and Co in 2*a* at (0, 0, 0) and Sb in 2*c* at (1/3, 2/3, 1/4).

2.2. Elastic properties

The elastic stiffness tensor is related to the stress tensor and the strain tensor by Hooke's law. The elastic constants are calculated as the second derivatives of the internal energy with respect to the strain tensor. The elastic stiffness tensor c_{ijkl} can be expressed as [27,28]

$$C_{ijkl} = \left(\frac{\partial \sigma_{ij}(x)}{\partial e_{kl}}\right)_X \tag{1}$$

with e_{kl}, σ_{ij}, X, x are Eulerian strain tensor, applied stress, the coordinates before and after deformation, respectively. Since the stress and strain tensors are symmetric, the most general elastic stiffness tensors have only 21 non-zero independent components. For a cubic system, the number of the independent elastic constants reduces to three (C_{11}, C_{12}, and C_{44}). These elastic constants can be determined by computing the stress generated by applying a small strain to an optimized unit cell [29]. In practice, the maximum strain amplitude was set from −0.003 to 0.003 with the step of 0.001, all forces on atoms are converged to less than 0.006 eV/Å. Before the calculations of the elastic constants of different pressures, a corresponding equilibrium structure should be obtained using the above BFGS algorithm.

The adiabatic bulk B and the shear modulus G for a cubic crystal structure are taken as [30,31]:

$$B_V = \frac{C_{11} + 2C_{12}}{3}, \tag{2}$$

$$G_V = \frac{1}{5}(2C + 3C_{44}), \tag{3}$$

$$B_R = \frac{C_{11} + 2C_{12}}{3}, \tag{4}$$

$$G_R = \frac{15}{(6/C + 9/C_{44})}, \tag{5}$$

where

$$C = \frac{1}{2}(C_{11} - C_{12}). \tag{6}$$

The arithmetic average of the Voigt and the Reuss bounds is commonly used to estimate the elastic moduli of polycrystals. In the terms of the Voigt–Reuss–Hill approximations [32]

$$B = \frac{B_V + B_R}{2}, \tag{7}$$

$$G = \frac{G_V + G_R}{2}, \tag{8}$$

Young's modulus E and Possion's ratio σ can be calculated by

$$E = \frac{9BG}{3B + G}, \quad \sigma = \frac{1}{2}\left(1 - \frac{E}{3B}\right) \tag{9}$$

The Debye temperature may be estimated from the average sound velocity V_m [33]

$$\Theta = \frac{\hbar}{k}\left[\frac{3n}{4\pi}\left(\frac{N_A \rho}{M}\right)\right]^{1/3} V_m \tag{10}$$

where $\hbar$ is Planck's constants, κ Boltzmann's constant, N_A Avogadro's number, n the number of atoms per formula unit, M the molecular mass per formula unit, ρ the density, and V_m is obtained from [33]:

$$V_m = \left[\frac{1}{3}\left(\frac{2}{V_s^3} + \frac{1}{V_l^3}\right)\right]^{-1/3} \tag{11}$$

where V_s and V_l are the average shear and longitudinal sound velocities, respectively. Their probable values can be calculated from Navier's equations as following [34]:

$$V_s = \sqrt{\frac{G}{\rho}}, \quad V_l = \sqrt{\frac{(B + 4/3G)}{\rho}} \tag{12}$$

Table 1
Lattice constants (Å), cell volume V_0 (Å^3) per formula unit, equilibrium energy E_0 (eV) per formula unit, bulk modulus B_0 (GPa) and its pressure derivative B_0' of the cubic and hexagonal structures CoVSb at 0 GPa and 0 K.

	Cubic CoVSb (primitive cell)				Hexagonal CoVSb (primitive cell)				
	Para[a]	Ferro[b]	Expt.	Others	Configuration I		Configuration II		Expt
					Para[a]	Ferro[b]	Para[a]	Ferro[b]	
a	4.120	4.126	4.103 [16] 4.103 [17]	4.108 [7]	4.365	4.376	4.493	4.493	4.200 [16]
c	–	–	–	–	5.359	5.365	5.254	5.255	5.398 [16]
V_0	49.075	49.685	48.828 [16] 48.828 [17]	49.005 [7]	44.214	44.489	45.927	45.928	41.240 [16]
B_0	156.100	162.950	–	–	175.480	148.170	147.900	148.510	–
B_0'	4.451	3.6269	–	–	4.397	5.0747	4.537	4.530	–

[a] Para denotes paramagnetic CoVSb.
[b] Ferro denotes ferromagnetic CoVSb.

3. Results and discussion

3.1. The ground state structure

Experimental structural information for cubic and hexagonal CoVSb was used as initial input [16]. In our calculations, both non-spin polarized (paramagnetic) and spin polarized (ferromagnetic) cases were considered. For spin-polarized case, formal high spin, three and two were set for Co and V atoms, respectively. We optimized the lattice geometry and ionic positions to get the fully stable geometry structures of the cubic and hexagonal CoVSb in the two cases. No constraints were imposed, the lattice parameters (a for cubic CoVSb or a and c for hexagonal CoVSb) were optimized simultaneously. Through the method, we can obtain the equilibrium lattice parameters and corresponding primitive cell volume V, equilibrium energy and enthalpy at arbitrary pressure for the cubic and hexagonal CoVSb. To get the zero pressure bulk modulus and its pressure derivative, we optimized the cubic and hexagonal geometry structures in the pressure range from −20 GPa to 100 GPa. A series of equilibrium cell volumes (from 1.3 V_0 to 0.7 V_0, where V_0 is zero-pressure equilibrium primitive cell volume) and corresponding equilibrium energy were drawn. Then, these V–E data for both the non-spin polarized and spin polarized cases were respectively fitted to the spinodal equation of state (EOS) proposed by García Baonza et al. [35]:

$$V = V_{sp} \exp\left\{-\left[\frac{K^*}{1-\beta}\right](P - P_{sp})^{1-\beta}\right\} \tag{13}$$

where

$$V_{sp} = V_0 \exp\left\{\frac{\beta}{(1-\beta)B_0'}\right\} \tag{14}$$

In Eq. (13), P_{sp} and V_{sp} are the spinodal pressure and volume, respectively. The fitting parameters are P_{sp}, K^*, and β (it is customary to use $\beta = 0.85$), and

$$B_0 = [K^*]^{-1}(-P_{sp})^{\beta} \tag{15}$$

$$B_0' = (-P_{sp})^{-1}\beta B_0 \tag{16}$$

The obtained structural parameters, zero pressure bulk modulus and its pressure derivative are presented in Table 1, together with the available experimental and theoretical data. It is seen that the lattice a and cell volume V_0 (per unit cell) for both cubic and hexagonal CoVSb are a little bigger than the experimental data, which may due to the fact that GGA calculations usually overestimate structural parameters. When cubic CoVSb transforms to hexagonal CoVSb with atomic configurations I or II, cell volume V_0 decreases. But this does not lead to the greater bulk modulus shown in the table (except for hexagonal CoVSb with atomic configuration I in non-spin polarized case), which may be due to reduced bond strength because of partial increased bond lengths [16] on the hexagonal CoVSb.

On the other hand, the obtained equilibrium energies (per unit cell) have the order: E(cubic ferromagnetic) < E(cubic paramagnetic) < E(hexagonal ferromagnetic with atomic configuration I) < E(hexagonal paramagnetic with atomic configuration I) < E(hexagonal ferromagnetic with atomic configuration II) ≈ E(hexagonal paramagnetic with atomic configuration II). The cubic ferromagnetic CoVSb has the lowest energy at 0 K and 0 GPa in all considered configurations and is the most stable structure, as is consistent with the experimental discoveries [15,16] that CoVSb is cubic ferromagnetic structure at low temperature and low pressure. For hexagonal CoVSb, ferromagnetic structure with atomic configuration I has the lowest energy. Combining the crystal structure data in Table 1, it is accepted that the ferromagnetic CoVSb with atomic configuration I is the most possible circumstance in all considered hexagonal configurations. This will be further confirmed by the research of pressure-induced phase transition in Section 3.4. We also note that hexagonal CoVSb with atomic configuration II has almost same lattice constants and equilibrium energies in non-spin polarized and spin-polarized cases, which mean that the hexagonal CoVSb with atomic configuration II is paramagnetic structure. These characters also can get supports from the density of state (DOS) of alpha and beta in Section 3.3. Thus, if there are no especial illustrations in the following work, for the cubic CoVSb and hexagonal CoVSb with atomic configuration I, only spin polarized (ferromagnetic) cases are considered; for the hexagonal CoVSb with atomic configuration II, only non-spin polarized (paramagnetic) case is considered.

3.2. Elastic properties

The elastic constants of cubic CoVSb under some pressures are listed in Table 2. It is noted that C_{ij} increases roughly with the enhancement of pressure. When the applied pressure is from 0 GPa to 15 GPa, the change ratios ($\Delta C/\Delta P$) of C_{11}, C_{12}, and C_{44} are 653%, 420%, and 13%, respectively. The change of C_{11} is a little more sensitive to pressure than others, while C_{44} is the most unresponsive one.

Elasticity, being a fourth-rank tensor, for a cubic crystal, is anisotropic. This is conveniently judged by the dimensionless shear

Table 2
Elastic constants C_{ij} (GPa) and elastic anisotropic factor of cubic CoVSb under pressure P (GPa) at 0 K.

P	C_{11}	C_{12}	C_{44}	A
0	241	91	57	−0.149
5	273	111	55	−0.190
10	307	132	58	−0.192
15	339	154	59	−0.197

Table 3
Bulk modulus B (GPa), shear modulus G (GPa), Young's modulus E (GPa), the Poisson's ratio σ; Shear, longitudinal and average sound velocities V_s, V_l, V_m (m/s), and Debye temperature Θ (K), of 'half-Heusler' cubic CoVSb under pressure P (GPa) at 0 K.

P	B	G	E	σ	V_s	V_l	V_m	Θ
0	141	64	165	0.304	2866	5400	3203	374
5	165	65	170	0.327	2834	5598	3177	375
10	190	69	183	0.339	2883	5850	3230	385
15	216	71	196	0.352	2895	6062	3256	391

anisotropic factor in the following relationship [29]:

$$A = \frac{2C_{44} + C_{12} - C_{11}}{C_{11}}. \quad (17)$$

Through the calculated elastic constants listed in Table 2, we can obtain the elastic anisotropic parameter A at different pressures. The results are also shown in Table 2. It is found that the anisotropic parameter A of the 'half-Heusler' cubic CoVSb remains negative in the entire range of pressure studied and increases with increasing pressure. When the applied pressure increases from 0 to 5 GPa, the elastic anisotropy increases sharply with pressure; but further increasing pressure, the elastic anisotropy increases slowly.

The calculated bulk modulus B, shear modulus G, Young's modulus E, Poisson's ratio σ, the shear, longitudinal and average sound velocities (V_s, V_l, V_m), and Debye temperature Θ under different pressures are listed in Table 3. The obtained zero-pressure bulk modulus is a little smaller than that from the front spinodal equation of state (EOS). It is also seen that all these physical quantities present the increasing change tendency with increasing pressure. An interesting change is the change of Poisson ratio. According to Frantsevich's rule [36], the critical value of Poisson ratio of a material is 1/3. For brittle materials, the Poisson ratio is less than 1/3, and values larger than 1/3 can be regarded as ductile materials. At 0 GPa or a lower pressure, the 'half-Heusler' cubic CoVSb alloy is brittle; however, at higher pressure, it will become more ductile.

As is known, for a cubic crystal, the mechanical stability under isotropic pressure is judged from the following conditions [37]:

$$\tilde{C}_{44} > 0, \quad \tilde{C}_{11} > |\tilde{C}_{12}|, \quad \tilde{C}_{11} + 2\tilde{C}_{12}) > 0 \quad (18)$$

where

$$\tilde{C}_{\alpha\alpha}c_{\alpha\alpha} - P(a = 1, 4), \quad \tilde{C}_{12} = c_{12} + P, \quad \tilde{C}_{13} = c_{13} + P. \quad (19)$$

The elastic constants in Table 2 satisfy all of these conditions. Therefore, the cubic 'half-Heusler' alloy CoVSb is mechanical stable at pressure up to 15 GPa.

3.3. Electronic band structures and densities of states

The calculated band structures of alpha and beta at 0 GPa for the cubic CoVSb are shown in Fig. 3. Clearly, the cubic CoVSb should attribute to half-Heusler alloy because two bands cross the Fermi level in one spin direction and an indirect band gap with 0.87 eV is presented on the other spin direction. The conclusion is in good agreement with other theoretical results [7,19–21]. In Fig. 4, band structures at 5, 10, 15 GPa for the cubic CoVSb in spin down (Beta) case are also presented. It is seen that band gap increases (0.98 at 5 GPa and 1.12 eV at 10 GPa) with pressure up to 10 GPa; this is an unusual consequence, which expects further research. But semiconductor character loses with pressure up to 15 GPa.

To elucidate some changes of electronic properties on different crystal structures, we also calculated the density of state (DOS) of alpha and beta for the cubic CoVSb and hexagonal CoVSb with atomic configuration I and II, which are shown in Fig. 5. The calculated density of states for the cubic CoVSb keeps half-Heusler and ferromagnetic characters and is consistent with the above band

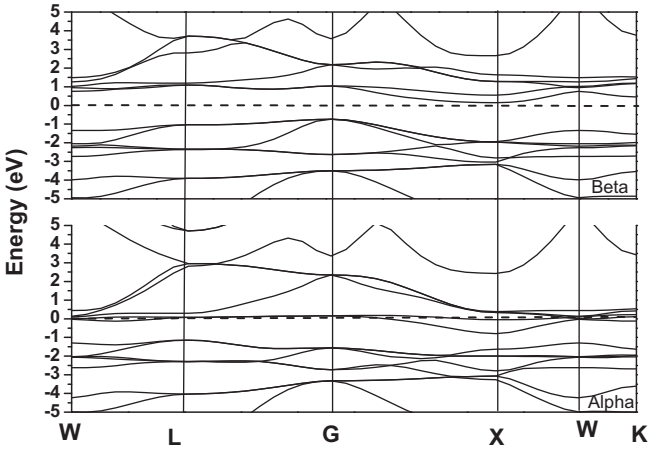

Fig. 3. Electronic band structures of alpha and beta at 0 GPa for cubic CoVSb. The Fermi level is set at zero.

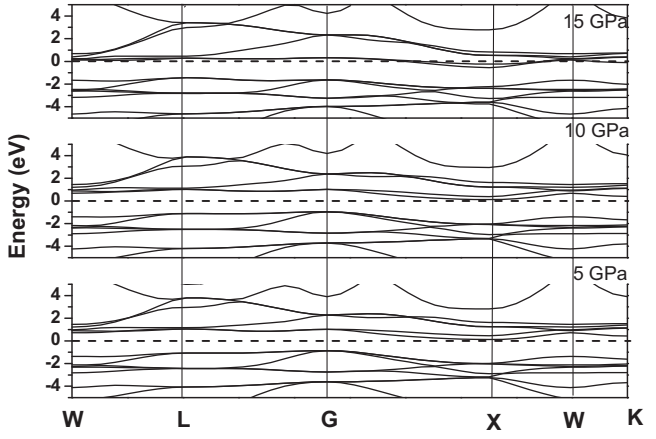

Fig. 4. Electronic band structures of beta at 5, 10, 15 GPa for cubic CoVSb. The Fermi level is set at zero.

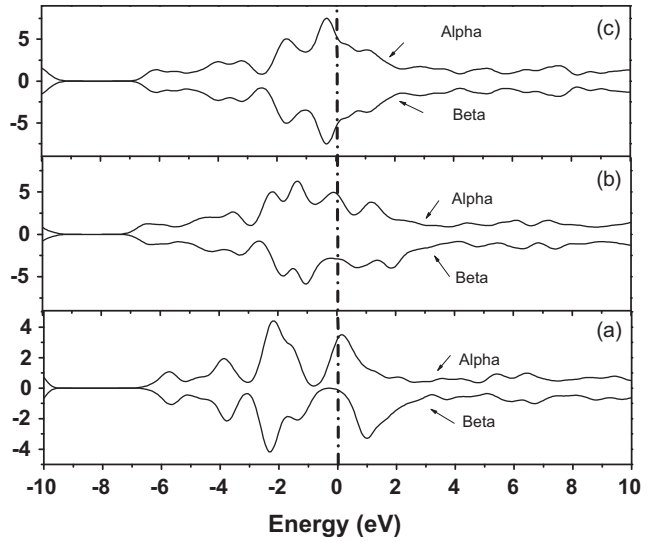

Fig. 5. Density of states (DOSs) of alpha and beta CoVSb at 0 GPa and 0 K: (a) cubic CoVSb; (b) hexagonal CoVSb with atomic configuration I; (c) hexagonal CoVSb with atomic configuration II. The Fermi level is set at zero.

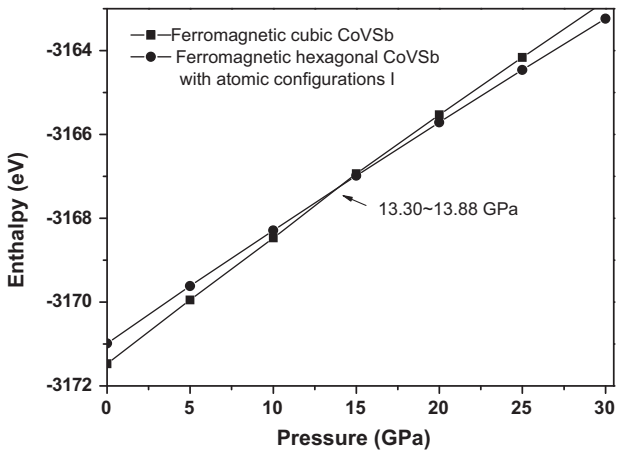

Fig. 6. Enthalpy as a function of pressure for the ferromagnetic cubic CoVSb and ferromagnetic hexagonal CoVSb with atomic configuration I at 0 K.

structure calculations. When the cubic CoVSb transforms to hexagonal CoVSb with atomic configuration I, the half-Heusler character loses but ferromagnetic character keeps. If it transforms to hexagonal CoVSb with atomic configuration II, both the half-Heusler and ferromagnetic characters lose.

3.4. Pressure-induced phase transition at 0 K

The transition pressure can be estimated from the usual condition of equal enthalpies ($H = E + PV$). For every CoVSb structure configuration (including ferromagnetic cubic CoVSb, ferromagnetic hexagonal CoVSb with atomic configuration I and paramagnetic hexagonal CoVSb with atomic configuration II), we performed the structural optimization at different pressures to acquire the corresponding enthalpies. The variations of the enthalpies for CoVSb in the three structures as a function of pressure at 0 K are given in Figs. 6 and 7.

The intersections of the enthalpy-pressure curves of different structures show the transition pressure from the ferromagnetic cubic CoVSb to the ferromagnetic hexagonal CoVSb with atomic configuration I is about 13.5 GPa; the transition pressure from the ferromagnetic cubic CoVSb to the paramagnetic hexagonal CoVSb with atomic configuration II is about 78.0 GPa. We noted that the difference of transition pressures from the ferromagnetic cubic CoVSb to two kinds of different hexagonal CoVSb configurations

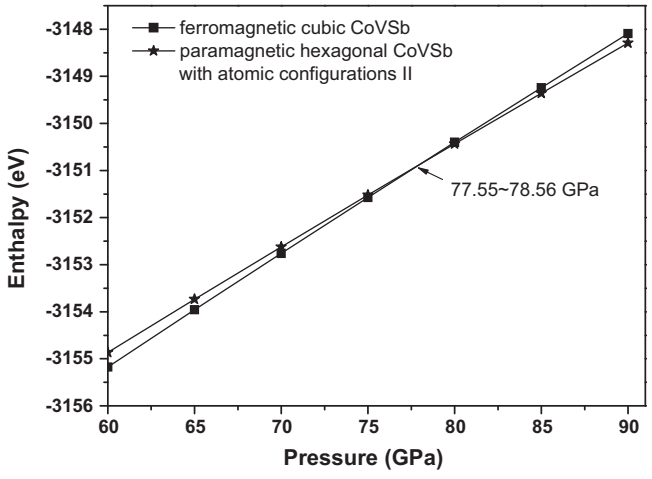

Fig. 7. Enthalpy as a function of pressure for the ferromagnetic cubic CoVSb and paramagnetic hexagonal CoVSb with atomic configuration II at 0 K.

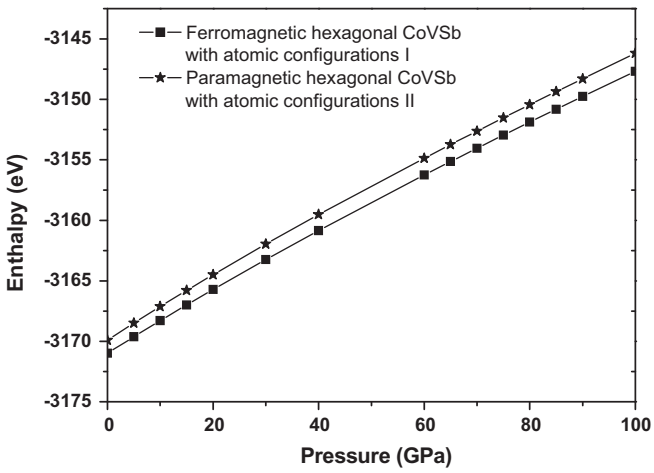

Fig. 8. Enthalpy as a function of pressure for ferromagnetic hexagonal CoVSb with atomic configuration I and paramagnetic hexagonal CoVSb with atomic configuration II at 0 K.

is not small, rather than great. On the other hand, the enthalpies of the ferromagnetic hexagonal CoVSb with atomic configuration I are always lower than that of the paramagnetic hexagonal CoVSb with atomic configuration II in the studied pressure range, and their difference value has the trend of becoming larger and larger with increasing pressure (Fig. 8). These results show that (i) the ferromagnetic hexagonal CoVSb with atomic configuration I is more stable at any pressure, (ii) it is difficult to realize the phase transition from the ferromagnetic hexagonal CoVSb with atomic configuration I to the paramagnetic hexagonal CoVSb with atomic configuration II with increasing pressure. With the analysis of the front ground-state structures, we can safely say hexagonal CoVSb with atomic configurations I and II are not at an equal position. The hexagonal CoVSb with atomic configuration I should be dominant atomic configuration. While in experiment, Noda et al. [16] pointed out it is expected that V and Co atoms randomly distribute on both 2(a) and 2(d) sites (atomic configurations I and II) in the hexagonal structure. As is not consistent with our theoretical results, further experiments are desired for the clarification of the question. As far as the transition pressure is concerned, the obtained theoretical results at 0 K show that the transition pressure improves when temperature decreases, in term that phase transition of the 'half-Heusler' cubic CoVSb occurs at 5 GPa and 1200 K from the experimental discovery of Noda et al. [16].

4. Summary

The structural, elastic properties and the pressure-induced phase transition of 'half-Heusler' alloy CoVSb at 0 K have been extensively studied using the pseudopotential plane wave method. The ground-state parameters, such as lattice constants, bulk modulus and its pressure derivative for cubic and hexagonal CoVSb were predicted and compared with the available experimental and theoretical data. We have additionally predicted the elastic constants of the 'half-Heusler' cubic CoVSb alloy under pressure and the pressure-induced phase transition for the fist time. From the obtained elastic constants, we have analyzed its mechanical stability, anisotropic behavior and drawn some important physical quantities at different pressures, such as bulk modulus B, Poisson's ratio σ and Debye temperature Θ. The research of phase transition and the calculations of electronic structures show the 'half-Heusler' cubic CoVSb transforms to normal hexagonal CoVSb with atomic configurations I and II at about 13.5 and 78.0 GPa, respectively at 0 K. Combining the analysis of ground-state structures, it is con-

cluded that the 'half-Heusler' cubic CoVSb mainly transforms to hexagonal CoVSb with atomic configuration I at a relative lower pressure.

Acknowledgments

The authors thank the support by the National Natural Science Foundation of China (Grant No. 10776022), by the Specialized Research Fund for the Doctoral Program of Higher Education (Grant No. 20090181110080), and by the Open Fund of State Key Laboratory Breeding Base of Green Chemistry-Synthesis Technology, Zhejiang University of Technology (Grant No. GCTKF2010017). We also acknowledge the support for the computational resources by the State Key Laboratory of Polymer Materials Engineering of China in Sichuan University.

References

[1] R.A. de Groot, F.M. Mueller, P.G. van Engen, K.H.J. Buschow, Phys. Rev. Lett. 50 (1983) 2024.
[2] K.E.H.M. Hanssen, P.E. Mignarends, Phys. Rev. B 34 (1986) 5009.
[3] M.C. Kautzky, F.B. Mancoff, J.F. Bobo, P.R. Johnson, R.L. White, M.B. Clemens, J. Appl. Phys. 81 (1997) 4026.
[4] J.S. Moodera, L.R. Kinder, T.M. Wong, R. Merservey, Phys. Rev. Lett. 74 (1995) 3273.
[5] S. Kammerer, S. Heitmann, D. Meyners, D. Sudfield, A. Thomes, A. Hutten, G. Reiss, J. Appl. Phys. 93 (2003) 7945.
[6] G.A. Prinz, J. Magn. Magn. Mater. 200 (1999) 57.
[7] S. Ishida, T. Masaki, S. Fujii, S. Asano, Physica B 239 (1997) 163.
[8] D. Junga, H.J. Koob, M.H. Whangbo, J. Mol. Struct. (Theochem.) 527 (2000) 113.
[9] O.I. Bodak, B.V. Padlyak, Yu.V. Stadnyk, J. Pierre, A.V. Tkachuk, L.P. Romaka, Yu.K. Gorelenko, J. Alloys Compd. 317–318 (2001) 357.
[10] M. Zhang, Z. Liu, H. Hu, Y. Cui, G. Liu, J. Chen, G. Wu, Y. Sui, Z. Qian, Z. Li, H. Tao, B. Zhao, H. Wen, Solid State Commun. 128 (2003) 107.
[11] L. Jodin, J. Tobola, P. Pecheur, H. Scherrer, Phys. Rev. B 70 (2004) 134426.
[12] V. Ksenofontov, G. Melnyk, M. Wojcik, S. Wurmehl, K. Kroth, S. Reiman, P. Blaha, C. Felser, Phys. Rev. B 74 (2006) 134426.
[13] C.S. Lue, C.F. Chen, F.K. Chiang, M.W. Chu, Phys. Rev. B 80 (2009) 184207.
[14] P.I. Kripyakevich, V.Ya. Markiv, Dopou. Akad. Nauk Ukr. RSR 12 (1963) 1606.
[15] M. Terada, K. Endo, Y. Fujita, R. Kimura, J. Phys. Soc. Jpn. 32 (1972) 91.
[16] Y. Noda, M. Shimada, M. Koizumi, Inorg. Chem. 18 (1979) 1318.
[17] K. Kaczmarska, J. Pierre, J. Beille, J. Tobola, R.V. Skolozdra, G.A. Melnik, J. Magn. Magn. Mater. 187 (1998) 210.
[18] L. Heyne, T. Igarashi, T. Kanomata, K.U. Neumann, B. Ouladdiaf, K.R.A. Ziebeck, J. Phys.: Condens. Matter 17 (2005) 4991.
[19] J. Tobola, J. Pierrez, S. Kaprzyky, R.V. Skolozdrax, M.A. Kouacouz, J. Phys.: Condens. Matter 10 (1998) 1013.
[20] I. Galanakis, P.H. Dederichs, Phys. Rev. B 66 (2002) 134428.
[21] B.R.K. Nanda, I. Dasgupta, J. Phys.: Condens. Matter 15 (2003) 7307.
[22] M.C. Payne, M.P. Teter, D.C. Allen, T.A. Arias, J.D. Joannopoulos, Rev. Mod. Phys. 64 (1992) 1045.
[23] V. Milman, B. Winkler, J.A. White, C.J. Packard, M.C. Payne, E.V. Akhmatskaya, R.H. Nobes, Int. J. Quant. Chem. 77 (2000) 895.
[24] J.P. Perdew, K. Burke, Ernzerhof, Phys. Rev. Lett. 77 (1996) 3865.
[25] D. Vanderbilt, Phys. Rev. B 41 (1990) 7892.
[26] B.G. Pfrommer, M. Côté, S.G. Louie, M.L. Cohen, J. Comp. Physiol. 131 (1997) 233.
[27] J. Wang, S. Yip, S.R. Phillpot, D. Wolf, Phys. Rev. B 52 (1995) 12627;
B.B. Karki, G.J. Ackland, J. Crain, J. Phys.: Condens. Matter 9 (1997) 8579.
[28] D.C. Wallace, Thermodynamics of Crystals, Wiley, New York, 1972.
[29] B.B. Karki, L. Stixrude, S.J. Clark, M.C. Warren, G.J. Ackland, J. Crain, Am. Miner. 82 (1997) 51;
R.M. Wentzcovitch, N.L. Ross, G.D. Price, Phys. Earth Planet. Int. 90 (1995) 10.
[30] D.W. Voigt, Lehrbuch der Kristallphysik, Leipzig, Taubner, 1928.
[31] A. Reuss, Z. Angew, Math. Mech. 9 (1929) 55;
L.L. Sun, Y. Cheng, G.F. Ji, J. At. Mol. Sci. 1 (2010) 143.
[32] R. Hill, Proc. Soc. Lond. A 65 (1952) 350.
[33] O.L. Anderson, J. Phys. Chem. Solids 24 (1963) 909.
[34] E. Schreiber, O.L. Anderson, N. Soga, Elastic Constants and their Measurements, McGraw-Hill, New York, 1973.
[35] V. García Baonza, M. Cáceres, J. Núñez, Phys. Rev. B 51 (1995) 28.
[36] I.N. Frantsevich, F.F. Voronov, S.A. Bokuta, in: I.N. Frantsevich (Ed.), Elastic Constants and Elastic Moduli of Metals and Insulators Handbook, Naukova Dumka, Kiev, 1983, p. 60.
[37] G.V. Sin'ko, N.A. Smirnov, J. Phys.: Condens. Matter 14 (2002) 6989.